# Experimental investigation of reinforced concrete and hybrid fibre reinforced concrete shield tunnel segments subjected to elevated temperature

# Experimental Investigation of Reinforced Concrete and Hybrid Fibre Reinforced Concrete Shield Tunnel Segments Subjected to Elevated Temperature

Zhi-guo Yan [a,b,c] , Yi Shen [b,c] , He-hua Zhu [a,b,c], Xiao-jun Li [a,b,c], Yong Lu[d]

[a] *State Key Laboratory of Disaster Reduction in Civil Engineering, Tongji University, 1239 Siping Road, Shanghai 200092, China*

[b] *Department of Geotechnical Engineering, Tongji University, 1239 Siping Road, Shanghai 200092, China*

[c] *Key Laboratory of Geotechnical and Underground Engineering of the Ministry of Education, Tongji University, 1239 Siping Road, Shanghai 200092, China*

[d] *Institute for Infrastructure and Environment, School of Engineering, The University of Edinburgh, Edinburgh EH9 3JL, UK*

## Abstract

This paper presents a comprehensive experimental study on the comparative behaviour of the reinforced concrete (RC) and the hybrid fibre reinforced concrete (HFRC) shield TBM (Tunnel Boring Machine) tunnel lining segments exposed to fire. The tests were conducted using a newly developed test facility, which is capable of accommodating different mechanical loading and boundary conditions under different fire scenarios. Six RC segments and six HFRC segments were tested to the standard Eurocode HC (Hydrocarbon) curve, while two reference specimens, one for each type, were tested in ambient environment to provide benchmark data. Apart from the spalling resistance, the fire effects on the structural behaviour were investigated under different boundary conditions at the segment ends, including free sliding (no horizontal constraint), total horizontal restraint and controlled horizontal reaction. The vertical load capacities were investigated for both under-fire and post-fire scenarios. The experimental results revealed excellent spalling resistance in the HFRC segments under thermo-mechanical loading, while the RC segments exhibited better structural performance. A combination of RC design (with flexural reinforcement) and the use of hybrid fibres is deemed to be effective in providing good spalling resistance while at the same time ensuring a robust structural behaviour.

**Keywords:** Hybrid fibre reinforced concrete; Shield TBM tunnel; Lining segment; Fire test; Fire Resistance; Spalling

## 1. Introduction

Several major tunnel fire incidents have occurred in the past, for instance the Great Belt Tunnel fire in Denmark and the Mont-Blanc Tunnel fire in France and Italy. As noted in [1, 2], tunnel fire has characteristics of high peak temperature, rapid heating rate, long duration and a nonuniform temperature distribution inside the tunnel, thus tunnel fire can result in extensive and complex damages to concrete tunnel linings. Apart from deterioration in the mechanical properties of concrete due to high temperature, severe concrete spalling, as observed from the Mont-Blanc Tunnel fire, is also a major concern over the safety of concrete linings in the event of a tunnel fire. In the case of a metro shield TBM tunnel lining, further complexities arise from the configuration and joint connections of the shield lining segments.

A number of studies have been performed in recent years to examine fire damages to lining concrete and explore effective methods to prevent concrete thermal spalling. Caner and Böncü [3] performed hydrocarbon fire tests on an isolated K segment of a shield TBM tunnel in an unloaded state to investigate fire damage to the segment concrete. The study concluded that the deviation in safety factor of the TBM tunnel widened from soft soil to stiff soil condition for the hydrocarbon fire as the tunnel became more flexible. Yan et al. [4] carried out full-scale experiments to investigate fire damage to reinforced concrete (RC) metro shield TBM tunnel linings tested to a standard ISO834 fire curve. The results indicated that the temperature of the bottom reinforcement (bottom side heated) of the tunnel linings could exceed the failure temperature under the ISO834 curve with duration of 90 min. Yasuda et al. [5] conducted a full-scale fire test on fire protection measures for shield TBM tunnel composite segments under a RABT (Richtlinien fuer Ausstattung und Betrieb von Strassentunneln) fire curve. It was found that spalling of concrete occurred and it reached up to 60 mm when there was no fire protection on the surface.

Steel fibre reinforced concrete (SFRC) has been increasingly adopted in tunnel linings, as evidenced in several precast SFRC tunnels built around the world [6, 7]. Adding steel fibres to

tunnel segments can effectively improve the tensile strength and ductility, mitigate cracking at ambient temperature, and reduce the demand on steel reinforcing bars and the construction time [7, 8]. Compared to the RC tunnel lining, the presence of steel fibres also help control the propagation of cracking and thus improve the overall performance of concrete during and after exposure to sustained high temperatures [8, 9]. However, in a real tunnel fire, explosive spalling of tunnel lining can become significant in the first few minutes of fire [10]. It is generally recognised that spalling is closely related to the pore pressure buildup within the concrete and the mechanical stresses resulting from differential thermal expansion. Although steel fibres generally help to improve the stress condition, they tend to play a limited role in diffusing the pore pressure buildup in the rapidly heated regions of concrete [11]. Results from Chen and Liu [12] suggest that the presence of steel fibres may only delay the time before spalling occurs. Further studies by Yan et al. [8] on the behaviour of RC and steel fibre reinforced concrete (SFRC) lining segments exposed to a HC curve indicated that the RC segments performed better than segments with only SFRC in terms of the overall fire resistance.

Hybrid fibre reinforced concrete (HFRC) with a mixture of steel and polypropylene (PP) fibres has attracted a lot of attention more recently due to its apparent superior fire performance, particularly in mitigating spalling [13, 14]. PP fibres melt at approximately 160–170 ˚C; although this would result in a certain reduction in the residual strength of the composite material [13], the melting of the PP fibres within the heated concrete is believed to provide key mechanisms for the observed spalling resistance of the concrete. Among other theories (e.g. micro-fracture resulting from the expansion of the molten fibres [15]), melting of PP fibres is understood to produce new expansion channels and connect existing internal channels within concrete material [16], and consequently the accumulated water vapour can escape and the buildup of pore pressure inside concrete is alleviated, thus reducing the chance

of spalling [10, 15]. In a combined manner, the PP fibres can mitigate the spalling of concrete while the steel fibres provide high ductility and reduce crack propagation for the concrete [17]. This results in a desirable concrete thermal stability [8].

As far as the shield TBM tunnel lining is concerned, however, little has been reported in the literature so far regarding the effectiveness of using HFRC in the shield lining under elevated temperature. To fill in this gap, experimental data on the behaviour of the HFRC shield TBM tunnel linings in comparison with the RC linings under varying thermal-mechanical conditions are particularly needed.

In this paper, we present a comprehensive experimental study on the fire behaviour of RC and HFRC lining segments. The tests were carried out using a specially designed setup allowing a variety of boundary and fire conditions to be simulated. The spalling performance and the general effect of fire on the structural resistance in both types of the lining segments, with the elevation of temperature following the standard Eurocode HC curve, are examined. Beside the comparative observations, the experiments were also intended to provide useful experimental data for the development of improved analytical and numerical models for the coupled thermal-mechanical performance of the shield tunnel linings for engineering applications.

## 2. Experimental programme

### *2.1. Overview of Test specimens*

The test specimens represented shield lining segments at a reduced scale of about 1:3 with respect to the full-size lining units. The specimens were 300 mm in width and 120 mm in thickness, and their average radius was 990 mm. The size of the specimens allowed the composition of the materials in the actual construction to be maintained in the test specimens, thus avoiding any material scaling effect. **Fig.1** shows the dimensions and reinforcement details of the test lining segments. To preserve the key features of the actual metro shield

TBM tunnel lining, the hand hole, circumferential tongues, as well as grooves of the lining segment were retained and fabricated in the test models.

Two types of test lining segments, one using normal reinforced concrete (RC), and another using hybrid fibre reinforced concrete (HFRC), were investigated. The mix design for the plain concrete is shown in **Table 1**. Properties of the PP and steel fibres as provided by the manufacturer are presented in **Table 2** and **Table 3**, respectively. The PP fibres and the geometry of steel fibre are shown in **Fig.2**. The volume fraction of PP fibre and steel fibre was 2 kg/m$^3$ and 78 kg/m$^3$, respectively. The choice of a relatively high steel fibre volume was based on the consideration of ensuring an appropriate level of the flexural strength in the absence of any main reinforcement. According to some previous research on HFRC [18], the volumetric ratio of the steel fibres in the present study may still be considered to be within a practically acceptable limit. The measured standard cube strengths of the plain concrete and the hybrid fibre reinforced concrete at the ambient temperature, and measured at 28 days, are 69.8 MPa and 61.1 MPa, respectively. For the RC lining segments, the main reinforcing bars (hot-rolled) in the circumferential direction were installed with 15 mm concrete cover thickness (cf. **Fig.1**). For HFRC lining segments, no reinforcing bars were installed.

To ensure good and consistent quality in the preparation of the test specimens, all construction work, including the concrete mix design and production, casting and curing of the specimens, was carried out by a professional concrete plant. **Table 4** lists the concrete age of the specimens at the time of the experimental tests. The age of the specimens varied between approximately 6 and 18 months.

### *2.2. Test setup and procedure*

The overall test setup is illustrated in **Fig.3(a)-(b)**. The test system was developed at Tongji University for testing tunnel lining segments under both applied mechanical loads and elevated temperatures. This system consists of a mechanical loading frame and a furnace

powered by two combustors of industrial grade. The furnace can be controlled by a programmable system to achieve a desired heating up history. The maximum temperature in the furnace can reach 1200°C and the maximum heating rate is approximately 250 °C/min. A wide range of combinations of mechanical loading and fire scenarios, including high rate heating and high peak temperature in conjunction with diverse mechanical load patterns, can be achieved using this test system. In the present experiment, the furnace temperature was monitored and controlled to follow the standard Eurocode HC curve. Three K type thermocouples, which were threaded through the reserved holes in the cover insulation plates (**Fig.3(b)**), were installed at equal distance near the under-space of the segment to measure thermal exposure experienced by the specimens during testing.

The standard Eurocode HC curve which was adopted in the present study to simulate the heating phase [19] is expressed in Eq. (1):

$$T(t) = 20 + 1080\,(1 - 0.325\mathrm{e}^{-0.167t} - 0.675\mathrm{e}^{-2.5t}) \tag{1}$$

where $t$ is time (in minutes) and $T(t)$ is the gas temperature inside the furnace (in ˚C).

**Fig.3(b)** shows a fully insulated specimen mounted on top of the furnace. A closed heating chamber was formed by two removable cover insulation panels that were situated on the two opposite sides of the segment. Any gaps between the segment and the insulation panels were filled up with ceramic fibres. Hence, the heating condition was considered to represent a uniform, single-face heating of the tunnel linings in fire.

The peak temperature inside the furnace was set at 1100 ˚C, and the heating duration was 60 minutes. Subsequently, taking into account the cooling phase of an actual fire [20], the furnace was turned off, and the specimens were gradually cooled to the ambient temperature.

The mechanical loading and support conditions of the test segments were arranged with an aim to be representative of such conditions in a segment unit within a real shield tunnel lining structure, but in a relatively simplified manner. The general loading condition in a real

shield TBM tunnel structure may be characterized by inward external pressure exerted by the surrounding soil; however, the actual distribution of the pressure load is complicated and could vary from segment to segment. Therefore in the experiment the external pressure load was simplified into two point loads applied vertically at the one-third span locations of the segment. Depending on the location of a specific segment within a tunnel shield ring, the midspan of the segment could be subjected to positive moment (inner side in tension, occurring especially at the top and bottom regions of a tunnel ring) or negative moment (the two opposite side regions of a ring) in a service condition. To represent the effect of such conditions under elevated temperature, selected specimens, as will be described in detail later, were subjected respectively to an initial positive moment and negative moment. This was achieved by adjusting the horizontal forces which were applied at the two ends of the test segment via two horizontal actuators, as can be seen from **Fig.3(c)**.

The above considerations formed the primary basis for the experimental setup of the segment specimens and the loading and boundary conditions. With these conditions it is expected that the experiments will be able to serve as benchmark for validation of theoretical and numerical models concerning the fire performance of the lining segments, as well as providing a basis for the evaluation of the fire effects on real tunnel linings where knowledge about the specific loading conditions (e.g. axial force and initial bending moment) may be made available, for example through a separate tunnel structural analysis using FEM.

A schematic of the test specimen with variable boundary and loading conditions is shown in **Fig.3(c)**. Totally 14 segment specimens, including 7 pairs of RC and HFRC specimens correspondingly, were tested. For all the test specimens, the two vertical loads (each equal to $1/2\,P_v$) were applied by a single hydraulic actuator via a distribution beam; this allowed a simplified control of the applied load. The horizontal action applied at the specimen ends varied such that three different internal load conditions were simulated. As the horizontal

support force implies a "boundary condition" on an individual segment, hereinafter these three conditions are referred as three "BCs", namely, a) BC1: no horizontal load or free sliding (lower bound); b) BC2: controlled horizontal load to maintain a no sliding condition; and c) BC3: controlled horizontal load to result in a negative bending moment at the central section of the segment. This was achieved by keeping the horizontal load at a fixed ratio of 1:1.2 to the total vertical load, i.e. $P_v / P_h = 1.2$. Note that under both BC1 and BC2 the central section of the segment was in positive bending.

Four different combinations of fire and mechanical loading conditions (LC) were considered, namely:

(i) Loading Case 0 (LC-0): ambient temperature test. Two specimens, one for RC (designated as RC0) and one for HFRC (HFRC0), were tested under the basic boundary condition (BC1) to provide benchmark responses for comparison.

(ii) Loading Case 1 (LC-1): residual strength after exposure to fire. The test segments were first loaded mechanically to a prescribed initial (service) load level, and then subjected to a complete heating (following the standard Eurocode HC curve) and cooling cycle. After complete cooling, the specimens were loaded to failure, by increasing the vertical load, to investigate the ultimate strength after exposure to high temperature. Three pairs of specimens were tested with LC-1, under three different boundary conditions, respectively, including RC5/HFRC5 (under BC1); RC4/HFRC4 (under BC2); and RC6/HFRC6 (under BC3).

(iii) Loading Case 2 (LC-2): ultimate strength under fire. The test segments were heated following the standard Eurocode HC curve, without however any initial loads. After approximately 40 minutes of heating, the specimens were mechanically loaded to failure to investigate the ultimate strength under high temperature. Two pairs of specimens were subjected to LC-2 tests, including RC1/HFRC1 (under boundary condition BC1) and

RC2/HFRC2 (under BC3).

(iv) Loading Case 3 (LC-3): fire resistance test. The test specimens were first loaded to a high load level at about 80% of the estimated ultimate strength under ambient temperature, and they were then subjected to heating following the standard Eurocode HC curve and maintained at the highest temperature until the specimens failed by the combined temperature and mechanical loading effects. One pair of specimens, namely RC3 and HFRC3, were tested in this scenario under the basic boundary condition BC1.

A summary of the test conditions for all the specimens can be found in **Table 4.**

It should be mentioned that the test segments were not subjected to any constraints in the longitudinal direction (direction normal to the segment plane). This simplification drastically reduced the complexity of the whole test set-up, and was considered as representing a lower-bound longitudinal constraint in a real tunnel fire scenario. In fact, depending upon the spread of the fire and the distribution of the temperature field, the longitudinal constraint on an individual ring could vary from a minimal constraint, which would be the case of relatively localized fire so that the longitudinal expansion of the most affected ring is less constrained, to a practically fully restrained condition, which may be conceived in the case of spread fire so that a significant length of the tunnel is under similar thermal condition making each individual ring to be under almost a plane strain condition. Omitting the longitudinal constraint from adjacent rings would mean the concrete in compression is subjected to less confining stress, which implies lesser enhancement in the confined compressive strength; meanwhile it also implies a somewhat reduced degree of spalling due to a lower overall constraint on the thermal expansion. These implications are worth noting; nevertheless the experiments represent a clear (lower-bound) longitudinal constraint condition for benchmarking and comparison purposes.

### *2.3. Instrumentation*

The temperature distribution, midspan deflection, vertical load and horizontal forces at the support were measured in the lining segment tests (cf. **Fig.1**). Two measuring sections were arranged to measure the temperature within each test specimen. For each of the temperature measuring sections, five *K* type thermocouples were installed inside the specimens, at the positions of 10 mm, 30 mm, 60 mm, 90 mm and 120 mm from the heating surface of the linings, respectively (cf. **Fig.1**). To minimise the effect from heat radiation and concrete spalling or cracking on the accuracy of the temperature measurement, the thermocouples closest to the heating surface were installed at a depth of 10 mm into the concrete. The thermocouples had a minimal of 20 mm spacing along the width of the specimen to avoid interference between them. In addition, a K type thermocouple was installed on the extrados linings (120 mm from the heating surface).

The installation of the thermocouples was carried out by a carefully controlled procedure. Small holes (5 mm in diameter) were drilled first from the unexposed surface, one for each thermocouple. After cleaning these holes, a small amount of fine aluminium powder was injected into the bottom of the holes to ensure good heat conduction between the concrete and the thermocouples. The thermocouples were placed next, and the holes were then filled with cement paste.

LVDTs were employed to measure the midspan deflections, the auxiliary vertical deflections and horizontal displacements of the test lining segments. A load cell was placed under each hydraulic jack to ensure that a desired level of the applied load was maintained. In addition, the inner LVDT were placed under the horizontal jack to precisely measure the horizontal displacement of the support during the test (cf. **Fig.1**). The LVDTs were carefully protected from high temperature.

Other measurement instruments included an ultrasonic pulse velocity (UPV) test

instrument to examine the condition of concrete, and a non-destructive concrete moisture meter to measure the moisture content in the concrete of the specimens. A non-contact, high sensitivity infrared radiometer (MikroScan 7600PRO) was also used in this test for checking up the accuracy of temperature measurement. This device measures the infrared radiation emitted by the target surface and converts this radiation into a two-dimensional image related to the temperature distribution at the target surface.

## 3. Experimental results on temperature and spalling

### *3.1. Temperature results*

Typical measured furnace temperatures against time during both the heating and cooling phases for the RC6 and HFRC6 are shown in **Fig.4**. In fact, all the heating curves of the tests were very similar during the same time period.

**Fig.5** shows the concrete temperatures at various depths of the cross-section of RC6 and HFRC6, and these generally represent the temperature results in all RC and HFRC specimens, respectively. In both types of specimens, a temperature plateau, during which the temperature tended to hold, appears in the time-temperature curves when the temperature in the concrete at the measured locations reached around 100 ˚C (or slightly higher). This phenomenon may be attributed to the effect of evaporation of free water and chemically bonded water of the calcium silicate hydrate (C-S-H) of the lining concrete [21]. The concrete temperature then continued to increase until the endothermic evaporation terminated. Owing to the large thermal inertia, high thermal capacity and low heat conduction coefficient of concrete, the heat conduction within the lining segments were slow, resulting in significant dynamic nonlinear, nonuniform temperature distributions across the thickness of the linings in the fire tests. This variation trend is similar to the previous observations reported in the literature [4, 8, 22].

### *3.2. Spalling and Cracking*

Spalling influences the performance of concrete in various ways depending upon the applications. Above all, it can affect seriously the fire resistance of the structural element because extensive removal of concrete due to spalling exposes the core of the section, and the reinforcing steel, to a more rapid rise in temperature, and consequently reduces the load-bearing capacity.

The severity of spalling may be measured by both the spalling depth and the spalling spread area, which can be conveniently illustrated by spalling contour plots. Typical spalling contours after the fire exposure for RC and HFRC segments are shown in **Fig.6. Fig.7** presents a pair of photographs showing different severity of spalling between RC and HFRC segments. It is worth noting that the spalling occurred from about the $30^{th}$ second to $120^{th}$ second after fire exposure. As almost no spalling occurred in the HFRC, only one HFRC specimen is shown here for a comparison.

In contrast to HFRC, extensive spalling occurred in the RC segments. Different RC specimens exhibit somewhat different patterns of spalling; however, such variation is deemed to be random and there was no evidence to suggest any close association with the different boundary conditions. As listed in **Table 4**, the maximum spalling area of HFRC segment was less than 0.5% of the inner face whereas the minimum spalling area of RC segment was 8.9%. During the tests, evaporation occurred and the vapour could be visibly observed to escape from the cracks of the lining segments.

In the HFRC specimens, the two types of fibres appeared to have worked effectively in protecting the specimens from explosive spalling and maintaining the surface integrity. Examination after the tests revealed that the steel fibres in the HFRC lining segments remained intact after exposure to high temperature, along with colour changes from a metallic color to a darker color which shows severe oxidation of steel fibres during heating.

**Fig.8** shows a comparison of the more detailed crack patterns between typical RC and HFRC specimens under LC1, which represents thermal-induced cracking under a service load condition. The crack widths on the side faces of all specimens were less than 1mm. However, the widths of the main cracks of RC segments on the heated face reached 2~3 mm (as a scale reference the diameter of the coin shown in the photos was 25 mm).

It should be noted that when the external load was increased to a level that caused flexural cracking, the steel fibres in HFRC specimens were exposed to fire directly, resulting in the softening of the steel fibres and consequently the failure of the entire specimen due to a lack of flexural reinforcement. This will be discussed further in Section 4.

## 4. Structural behaviour of tunnel segments and effects of fire

### *4.1 Structural behaviour under positive bending and fire effects*

The structural behaviour and the fire effects are firstly examined here on the RC specimens under the basic boundary condition BC1, i.e., sliding end supports representing a lower bound horizontal constraint. **Fig.9(a)** shows a comparison of the vertical load vs. mid-span deflection curves among the ambient temperature (LC0), post fire (LC1) and under-fire (LC2) loading cases. The three specimens under consideration are RC0, RC5 and RC1. It is noted that a "heating to failure" case (LC3) is also included in the graph, which will be explained later. The corresponding failure modes are presented in **Fig.10(a1)-(a3)**.

From the load-deflection curves it can be observed that the three specimens behaved similarly, suggesting that the fire effect was not significant in these specimens. A reduction of the maximum resistance at about 20% occurred in the two fire-exposed specimens as compared to the ambient test. However, this difference could be regarded as normal variation in these specimens with a non-ductile response. Indeed, all three specimens exhibited little ductility, and global failure occurred almost immediately after the maximum load was

attained.

Inspection of the failure patterns **(Fig.10(a1)-(a3))** reveals that all the three specimens exhibited a typical compressive bending failure over the mid-span region, with crushing of concrete occurring on the top (compressive) side of the segments, while major flexural cracks also developed. Based on the equilibrium and RC section analysis, it can be found that the tensile steel is slightly over-reinforced, and therefore the observed concrete compressive failure was not surprising. Such a governing mechanism also explains the less significant effect of fire on the overall behaviour and the maximum resistance of these specimens, as the critical compressive concrete on the top side of the specimens was essentially not affected by the fire.

It is worth highlighting that the above specimens were under a sliding support condition. It can be expected that when the horizontal constraint at the two end supports increases, the behaviour of the segment would be inclined further towards a compression-dominated bending mechanism because of the involvement of the axial compression. This was evidenced in specimen RC4, for which the vertical load vs. mid-span deflection curve is shown in **Fig.9(b)** and the failure pattern is given in **Fig.10(b)**. It can be seen that the specimen failed in a predominantly compressive manner, and as a result the maximum load resistance was about six times larger than the specimens under a sliding support condition, but became even more brittle. Although there was no direct comparison with an ambient test, based on the observations from the sliding RC specimens it may be reasonable to deduce that fire had an insignificant effect on the resistance of this specimen.

For the HFRC specimens under a sliding boundary condition, the vertical load vs. mid-span deflection curves are given in **Fig.11(a)**, and the corresponding failure modes are shown in **Fig.12(a1)-(a3)**. It is noted that the post fire case (HFRC5) failed during the cooling stage and so the curve is not included in **Fig.11(a)**; however the failure pattern was captured

as shown in **Fig.12(a3)**. Generally speaking, these specimens exhibited a less ductile behaviour; but unlike the RC specimens discussed earlier, the failure patterns in these HFRC specimens were apparently due to insufficient tensile capacity, i.e. an under-reinforced bending. Recall that the HFRC specimens had only fibre reinforcement and did not have main reinforcing steel bars. As a result, the specimens quickly reached an ultimate state when bending cracks developed due to the insufficient ability of the fibres in withstanding the tensile force under bending.

The above characteristic of the HFRC specimens under no horizontal constraint renders the segments to be structurally susceptible to the fire effect because the major positive bending cracks exposed the tension fibres near the bottom side to high temperature. This is evidenced by the marked reduction of the maximum vertical load in the under-fire test as compared to the ambient test, as well as the failure of HFRC5 specimen which was subjected to a constant initial load of 15% of the maximum ambient resistance but failed during the cooling phase. The seemingly increased ductility in the "under fire" test might be attributable to the softening of the steel fibres while being exposed to the high temperature.

A close-up inspection of the cracks during the ambient test, as shown in **Fig.13(a)**, suggests that the steel fibres were pulled out despite having originally hooked ends. This contributed to the insufficient tensile capacity on the tension side of the section. Under fire, however, the steel fibres crossing the main crack snapped because of softening under high temperatures; this resulted in an increased deformability but the maximum resistance was reduced considerably. The snap-rupture and melting of steel fibres was detectable at the main crack shown in **Fig.13(b)**.

When the HFRC segment was restrained horizontally at the segment end (BC2), as in the case of HFRC4, the bending moment in the middle portion of the segment was significantly reduced. At the same time, the bending capacity of the segment was increased because of the

increased axial compression. Therefore, the maximum vertical resistance increased considerably, as illustrated in **Fig. 11(b)** in comparison to **Fig. 11(a)**. The combination of axial force, bending and shear effects led eventually to a clear diagonal shear failure in the high shear region from the support to the first loading point, as shown in **Fig. 12(b)**. Comparing to RC4 which was under a similar boundary and fire condition, the failure mode in HFRC4 appeared to exhibit better deformability at the ultimate load level.

### *4.2 Structural behaviour and fire effects under negative (hogging) bending*

Two pairs of specimens, namely RC6-HFRC6 and RC2-HFRC2, were subjected to negative bending by a controlled horizontal action at the ends (BC3), and tested under two different fire scenarios, namely post-fire (LC1) and under-fire (LC2) respectively. In these specimens, the central section of the segment was kept under a negative (hogging) moment by maintaining a constant ratio of 1:1.2 between the horizontal support reaction to the vertical load, while the vertical loading increased. It should be pointed out that under this particular condition, although a hogging moment at the central section was maintained, the overall segment was subjected to relatively large compression along with significant shear force; therefore a somewhat complex failure process could be anticipated.

**Fig.14** presents the vertical load vs. mid-span deflection curves for all the hogging moment loading cases. The corresponding failure modes are shown in **Fig.15**.

The two RC specimens exhibited similar shapes in the vertical load – deflection curve (ignoring the beginning stage in the RC2 curve which was likely due to initial settlement). Both specimens experienced small vertical deflections during the first (elastic) stage of loading, which was quite expected given the internal force condition as already mentioned. However, the ultimate load of RC2 (under-fire test) was about 50% lower than that of RC6 (post-fire test) and the deformation capacity was also reduced significantly. From the failure

modes shown in **Fig.15(a) and (b)**, it is clear that the governing mechanism was due to relatively high shear, resulting eventually in shear failure near the loading point (towards the support). As the tension-shear cracks developed from the inner surface, both the reinforcing bars and the upper concrete along the shear crack were exposed to fire, leading to degradation of their strength under high temperature and hence a substantially reduced overall strength in the under-fire test as compared to the post-fire test, in which case the strength of the reinforcing bars recovered after cooling.

The load-deflection curves for the two HFRC segments are given in **Fig.14(b)**, and the failure patterns are shown in **Fig.15(c) and (d)**. Ignoring the initial settlement, the vertical deflection was also small at first (elastic) stage of loading, and tended to sway into the opposite (upward) direction (particularly in the case of post-fire test). The post-fire test specimen (HFRC6) failed in a rather brittle manner when the maximum load was attained, and the failure mode indicates that it was clearly a shear failure. The failure mode of the under-fire specimen (HFRC2) was somewhat peculiar, featuring a mixed bending failure in different regions of the specimen. This may be explained by the fact that, despite a hogging moment at the mid-span section, the controlled horizontal reaction and the vertical load ratio actually rendered the whole specimen to be under high compression (like an arch), while bending and shear failure could sway either way during the ultimate stage depending on the actual damage development under a significant compression state.

Because of a largely compressive mode of response until closer to the ultimate stage, the maximum vertical load capacity in the two HFRC specimens did not appear to have been affected significantly by the fire and different test scenarios. The under-fire test tends to exhibit an increased deformation capacity before failure, and this may be attributed to the softening of steel fibres at the major crack sections.

### *4.3 Fire endurance under large service load*

Two specimens (RC3 and HFRC3) were tested for fire endurance while being loaded at about 80% of their respective ultimate strength at ambient temperature. This load level is about 25%~40% higher than the typical service load level and was considered to represent an upper bound service load condition for the purpose of evaluating the fire resilience in a worst case load scenario. The support condition for both specimens was BC1, i.e., without any horizontal constraint. Thus, both specimens were subjected to a typical positive bending. Inspection before the fire test revealed visible flexural cracking in both specimens under the imposed vertical load.

When exposed to fire, specimen RC3 failed after approximately 42 minutes of heating, showing reasonable resilience against fire even under a high level of external load. Specimen HFRC3, on the other hand, failed after only two minutes of heating. The rapid failure of HFRC3 further demonstrated that the specimen with fibre reinforcement alone would possess little fire resistance due to a rapid loss of strength in the steel fibres at the flexural cracks when exposed to high temperature.

### *4.4 Influence of horizontal constraints on the fire effects*

The influence of different horizontal constraints at the segment ends on the fire effect is further examined by comparing the thermal induced deformations of the segments. **Fig.16** shows the measured mid-span deflections during both the heating and cooling phases for specimens under an initial service load but with three different horizontal support conditions, respectively, including RC5, RC4, RC6, and HFRC5, HFRC4 and HFRC6. Note that the deflections shown are the incremental deflections from the deformed positions after the initial loading.

Specimens RC5 and HFRC5, which had no horizontal constraint at the segment ends,

exhibited almost a linear increase of deflections during the heating phase (up to about 60 minutes). Specimen HFRC5 failed suddenly during the cooling phase, due apparently to the loss of strength of the tension fibres when the temperature inside the fracture zone reached a critical level. In specimen RC5, the mid-span deflections became almost stabilized during the cooling phase. This phenomenon is deemed to be a result of the combination of two opposite effects, i.e. increase of deformation on the deteriorating specimen under the same service load, and decrease of the thermal induced deflection as the temperature cooled down.

The thermal-induced mid-span deflections in the specimens with horizontal constraints were generally much smaller than the specimens on sliding supports. However, the variation of the deflections over time exhibited a generally similar pattern, with an increasing deflection during the heating phase and a more or less constant deflection during the cooling phase. The increase of the (upward) deflection in RC6 could be attributed to a combined thermal-mechanical effect under a hogging moment condition.

It is also instructive to examine the development of axial forces in the horizontally restrained specimens under elevated temperature. The measured fire-induced horizontal restraining force, as well as the bending moment at the central section, in specimens RC4 and HFRC4, are plotted as the functions of fire exposure time in **Fig.17**. Ignoring the irregularities in the first few minutes (which were primarily due to self-adjustment of the support fixture), a significant amount of horizontal restraining force developed during the heating phase in both specimens due to the restraining effect against thermal expansion. The increased horizontal reaction force reduced the (positive) bending moment from the service load in the mid-span, and in fact turned the initial sagging moment at the central section into hogging at the later part of the heating phase. Overall, the development of thermal-induced horizontal restraining force tends to result in an increasingly compression-dominated mode of response in the segments, and this phenomenon is noteworthy in the analysis of the real fire effects on tunnel

lining segments.

## 5. Conclusions

A comprehensive experimental investigation into the behaviour of the RC and HFRC shield TBM tunnel lining segments exposed to fire has been presented and discussed. The following conclusions may be drawn.

1) HFRC segments with a mixed use of steel and polypropylene fibres exhibited excellent spalling resistance. All the HFRC specimens experienced practically no spalling after exposure to the standard Eurocode HC curve. In contrast, extensive spalling occurred in all the RC segments without fibre reinforcement.
2) The RC segments exhibited good endurance under thermo-mechanical loading as compared to the particular HFRC segments where no flexural rebar was included. It is therefore reasonable to expect that a combination of both HFRC and RC design will enable robust fire performance in the tunnel lining segment in terms of spalling resistance as well as the general structural behaviour.
3) For the RC segments subjected to vertical loading with a minimum horizontal constraint at the segment ends, the behaviour of the segments was governed by positive bending (sagging); consequently, fire did not appear to affect significantly the structural behaviour. This was the case in both under-fire and post-fire scenarios. For the HFRC segments, however, the specimens exhibited little fire resistance under a similar flexural mode of response; as a matter of fact, the (steel) fibres easily snapped when exposed to high temperature, resulting in an abrupt failure of the segments.
4) When the segments were subjected to high horizontal constraints at the segment ends, significant axial compression force developed when the vertical load increased. This rendered the segments to behave in a compression-dominated mode of response. As a

result, the vertical load carrying capacity increased considerably. A similar increase in the vertical load carrying capacity was observed when the segments were subjected to controlled horizontal constraints resulting in a hogging moment at the centre of the segments. In these loading conditions, the fire effect on the RC segments tended to be more pronounced as compared with the situation under a flexural mode of response, such that a noticeable reduction in the vertical load carrying capacity occurred due to the deterioration of the compressive capacity of concrete under elevated temperature.

5) Significant lateral reaction forces were generated during heating when the horizontal movement at the segment ends was restrained. Under a given external vertical load, the lateral reaction force would partially offset the magnitude of the bending moment in the central region, but the presence of high compression increased the stress level which in turn tended to accelerate the deterioration of concrete under fire.

Further research is required to derive quantitative recommendations regarding the optimum dosage and the mixing ratio of the hybrid fibres, as well as detailed effects of the combined RC and HFRC designs to maximise the spalling resistance while maintaining a desirable structural behaviour of the tunnel lining segments when exposed to fire.

**Acknowledgements**

The authors acknowledge the financial supports from the National Basic Research Program of China (973 Program) (2011CB013800), the National Natural Science Foundation of China (51478345, 50808137), Shanghai Pujiang Program (14PJD034), and Research Program of State Key Laboratory for Disaster Reduction in Civil Engineering.

## References


[1] B.A. Schrefler, P. Brunello, D. Gawin, C.E. Majorana, Pesavento F. Concrete at high temperature with application to tunnel fire. Comput. Mech. 29 (2002) 43-51.

[2] A. Beard and R. Carvel. The handbook of tunnel fire safety. Thomas Telford, 2005.

[3] A. Caner, A. Böncü. Structural fire safety of circular concrete railroad tunnel linings. J. Struct. Eng.-ASCE 9 (2009) 1081-92.

[4] Z.G. Yan, H.H. Zhu, J.W. Ju, W.Q. Ding. Full-scale fire tests of RC metro shield TBM tunnel linings. Constr. Build. Mater. 36 (2012) 484-94.

[5] F. Yasuda, K. Ono, T. Otsuka. Fire protection for TBM shield tunnel lining. Tunn. Undergr. Sp. Tech. 19 (2004) 317.

[6] M. Vandewalle. Tunneling is an art. Zwevegem: NV Bekaert SA; 2005.

[7] A. Lau, M. Anson. Effect of high temperatures on high performance steel fibre reinforced concrete. Cem. Concr. Res. 36 (2006) 1698-1707.

[8] Z.G. Yan, H.H. Zhu, J.W. Ju. Behavior of reinforced concrete and steel fiber reinforced concrete shield TBM tunnel linings exposed to high temperatures. Constr. Build. Mater. 38 (2013) 610-618.

[9] F. Cheng, V. Kodur, T. Wang. Stress–strain for high strength concrete at elevated temperatures. J. Mater. Civ. Eng. 16 (2004) 84–90.

[10] M. Zeiml, D. Leithner, R. Lackner, A.M. Herbert. How do polypropylene fibers improve the spalling behavior of in-situ concrete? Cem. Concr. Res. 36 (2006) 929-942.

[11] M. Colombo, di M. Prisco, R. Felicetti. Mechanical properties of steel fibre reinforced concrete exposed at high temperatures. Mater. Struct. 43 (2010) 475-491.

[12] B. Chen, J. Liu. Residual strength of hybrid-fiber reinforced high strength concrete after exposure to high temperature. Cem. Concr. Res. 34 (2004) 1065–9.

[13] L.S. Suhaendi, T. Horiguchi. Effect of short fibers on residual permeability and mechanical properties of hybrid fibre reinforced high strength concrete after heat exposition. Cem. Concr. Res. 36 (2006) 1672-1678.

[14] M.R. Bangi, T. Horiguchi. Pore pressure development in hybrid fibre-reinforced high strength concrete at elevated temperatures. Cem. Concr. Res. 41 (2011) 1150-1156.

[15] P. Kalifa, G. Chéné, C. Gallé. High-temperature behaviour of HPC with polypropylene fibres: From spalling to microstructure. Cem. Concr. Res. 31 (2001) 1487-1499.

[16] P. Pliya, A.L. Beaucour, A. Noumowé. Contribution of cocktail of polypropylene and steel fibres in improving the behaviour of high strength concrete subjected to high temperature. Constr. Build. Mater. 25 (2011) 1926-1934.

[17] J.P.C. Rodrigues, L. Laím, A.M. Correia. Behaviour of fiber reinforced concrete columns in fire. Compos. Struct. 95 (2010) 1263-1268.

[18] N.A. Libre, M. Shekarchi, M. Mahoutian. Mechanical properties of hybrid fiber reinforced lightweight aggregate concrete made with natural pumice. Constr. Build. Mater. 25 (2011) 2458-2464.

[19] European Committee for Standardization (CEN). Eurocode 1: Actions on structures, EN 1991-1-2(2002).

[20] F. Wald, L. Simões da Silva, D.B. Moore, T. Lennon, M. Chladná, A. Santiago. Experimental behaviour of a steel structure under natural fire. Fire Saf. J 41 (2006) 509-22.

[21] G.A. Khoury, C.E. Majorana, F. Pesavento, B.A. Schrefler. Modelling of heated concrete. Mag. Concrete Res. 54 (2002) 77-101.

[22] M. Colombo, R. Felicetti. New NDT techniques for the assessment of fire-damaged concrete structures. Fire Saf. J. 42 (2007) 461-72.

**Table 1**

Mix design of concrete for the RC tunnel linings used in the tests

| Item | $kg/m^3$ |
|---|---|
| Portland cement | 386 |
| Aggregate | 1143 |
| Sand | 640 |
| Fly ash | 74 |
| Water | 155 |
| Admixture | 5.5 |

**Table 2**

Properties of polypropylene fibres

| Item | Value |
|---|---|
| Specific gravity | 0.91 |
| Length (mm) | 12 |
| Diameter (μm) | 18 |
| Tensile strength (MPa) | 365 |
| Elastic modulus (MPa) | 3300 |
| Melting point (˚C) | 160 |
| Ignition Point (˚C) | 590 |
| Alkali, acid and salt resistance | High |

**Table 3**

Properties of steel fibres

| Item | Value |
|---|---|
| Specific gravity | 7.8 |
| Length (mm) | 50 |
| Diameter (mm) | 0.9 |
| Tensile strength (MPa) | 1000 |
| Elastic modulus (MPa) | 200000 |
| Melting point (˚C) | 1370 |

**Table 4**

Summary of the test specimens, test programme and key results

| No. | Age (day) | BC [a] | Load case | Fire load | MC [b]-0 (%) | MC -1 (%) | MC-2 (%) | MC-3 (%) | MSD [c] (mm) | SA [d] (%) | SS [e] | $P_{max}$ [f] (kN) |
|---|---|---|---|---|---|---|---|---|---|---|---|---|
| RC0 | 321 | $P_{v0}$=0, $P_H$=0 (BC1) | LC-0 | - | 4.1 | - | - | - | - | - | - | $P_v$=74.5, $P_H$=0 |
| RC1 | 226 | $P_{v0}$=0, $P_H$=0 (BC1) | LC-2 | HC(60 minutes) | 3.9 | 0.2 | 0.1 | 0 | 6 | 16.9 | ++ | $P_v$=61, $P_H$=0 |
| RC2 | 251 | $P_{v0}$=0, $P_H$=0 (BC3) | LC-2 | HC(60 minutes) | 4.1 | 0.4 | 0.3 | 0 | 6 | 18.1 | ++ | $P_v$=240, $P_H$=200 |
| RC3 | 223 | $P_{v0}$=59.6 kN, $P_H$=0 (BC1) | LC-3 | HC(42 minutes) | 4.0 | 1.4 | 1.3 | 1.0 | 1 | 8.9 | + | $P_v$=59.6, $P_H$=0 |
| RC4 | 540 | $P_{v0}$=34.7 kN, $\delta_H$=0 (BC2) | LC-1 | HC(60 minutes) | 4.2 | 0.6 | 0.4 | 0 | 3 | 12.6 | + | $P_v$=369.81, $P_H$=271.56 |
| RC5 | 264 | $P_{v0}$=41 kN, $P_H$=0 (BC1) | LC-1 | HC(60 minutes) | 4.2 | 0.1 | 0 | 0 | 2 | 10.2 | + | $P_v$=61.9, $P_H$=0 |
| RC6 | 255 | $P_{v0}$=58.6 kN, $P_H$=48.8 kN (BC3) | LC-1 | HC(60 minutes) | 4.2 | 0.7 | 0.5 | 0.3 | 6 | 21.9 | +++ | $P_v$=465.6, $P_H$=388 |
| HFRC0 | 312 | $P_{v0}$=0, $P_H$=0 (BC1) | LC-0 | - | 4.2 | - | - | - | - | - | - | $P_v$=31, $P_H$=0 |
| HFRC1 | 176 | $P_{v0}$=0, $P_H$=0 (BC1) | LC-2 | HC(60 minutes) | 4.0 | 2.2 | 1.5 | 1.0 | <1 | <0.5 | - | $P_v$=22.6, $P_H$=0 |
| HFRC2 | 278 | $P_{v0}$=0, $P_H$=0 (BC3) | LC-2 | HC(60 minutes) | 4.0 | 2.1 | 1.5 | 1.2 | <1 | <0.5 | - | $P_v$=303.6, $P_H$=253 |
| HFRC3 | 282 | $P_{v0}$=23.8 kN, $P_H$=0 (BC1) | LC-3 | HC(1.9 minutes) | 4.6 | 4.6 | 4.6 | 4.5 | <1 | <0.5 | - | $P_v$=23.8, $P_H$=0 |
| HFRC4 | 271 | $P_{v0}$=13.8 kN, $\delta_H$=0 (BC2) | LC-1 | HC(60 minutes) | 4.3 | 2.2 | 1.9 | 1.8 | 0 | 0 | - | $P_v$=98.4, $P_H$=53.3 |
| HFRC5 | 269 | $P_{v0}$=16.4 kN, $P_H$=0 (BC1) | LC-1 | HC(60 minutes) | 4.2 | 2.0 | 1.9 | 1.4 | <1 | <0.5 | - | $P_v$=16.4, $P_H$=0 |
| HFRC6 | 269 | $P_{v0}$=45.4 kN, $P_H$=37.8 kN (BC3) | LC-1 | HC(60 minutes) | 4.1 | 1.5 | 1.4 | 1.1 | 1 | <0.5 | - | $P_v$=255.6, $P_H$=213 |

[a] BC-Boundary conditions, i.e. horizontal constraints (BC1 = free slide; BC2 = restrained; BC3 = controlled)

[b] MC- Moisture content:1-before heating, 2- outside surface after heating, 3- profile after heating, 4- inner surface after heating;

[c] MSD - Maximum explosive spalling depth

[d] SA - Spalling area

[e] SS - Spalling severity, +-Minor spalling, ++ Major spalling, +++Severe spalling

[f] Ultimate load of the lining segments

Figure

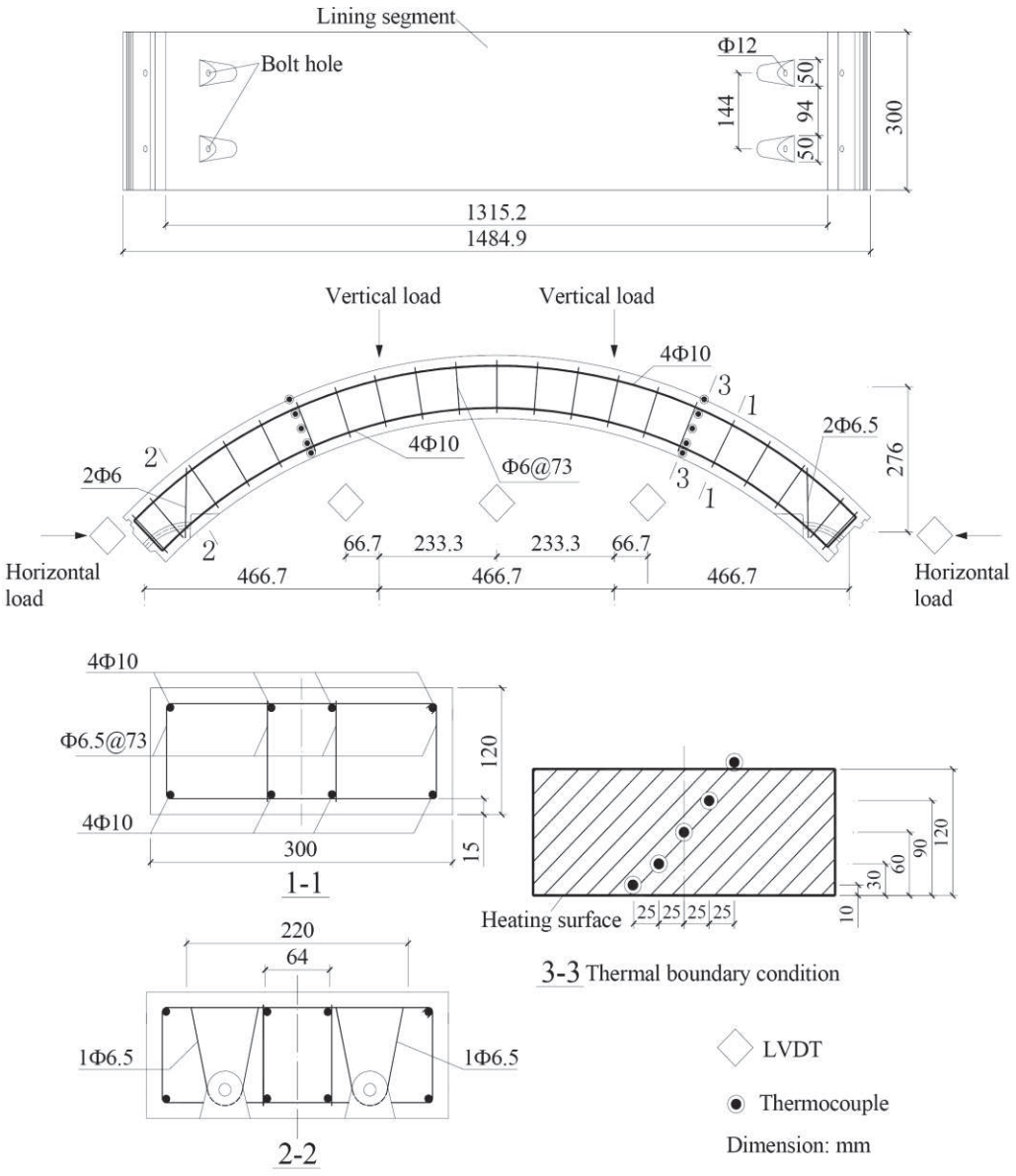


**Fig.1.** Geometry of the lining segments and reinforcement details of the RC specimens (Note: no reinforcing bars in HFRC specimens)

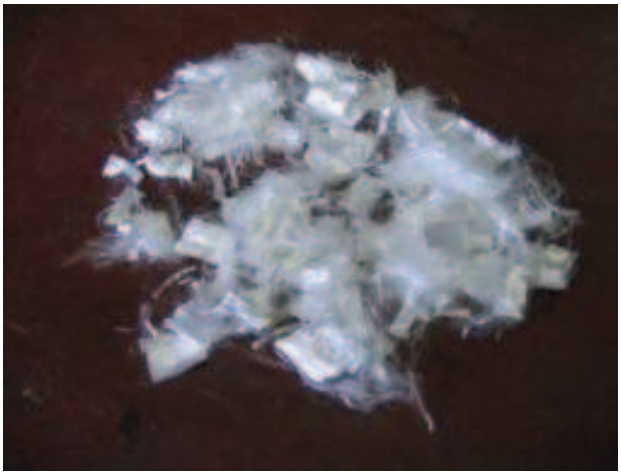

(a) polypropylene fibers

(b) steel fiber

**Fig.2.** Fibers used in this study

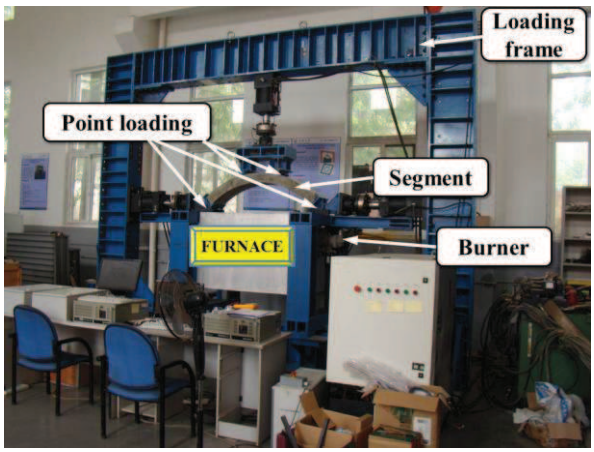


(a) Overall view of the test setup

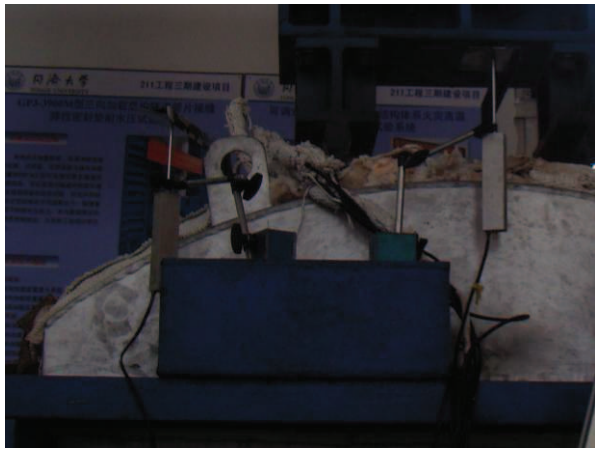

(b) Insulated specimen on top of furnace

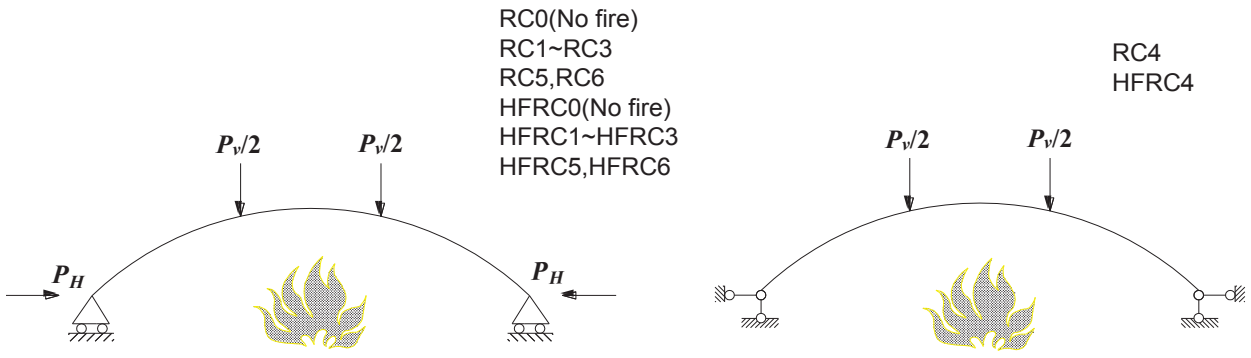


(c) Schematic of the test specimen with variable boundary and loading conditions

**Fig.3.** Test setup for combined mechanical and thermal loadings and support conditions

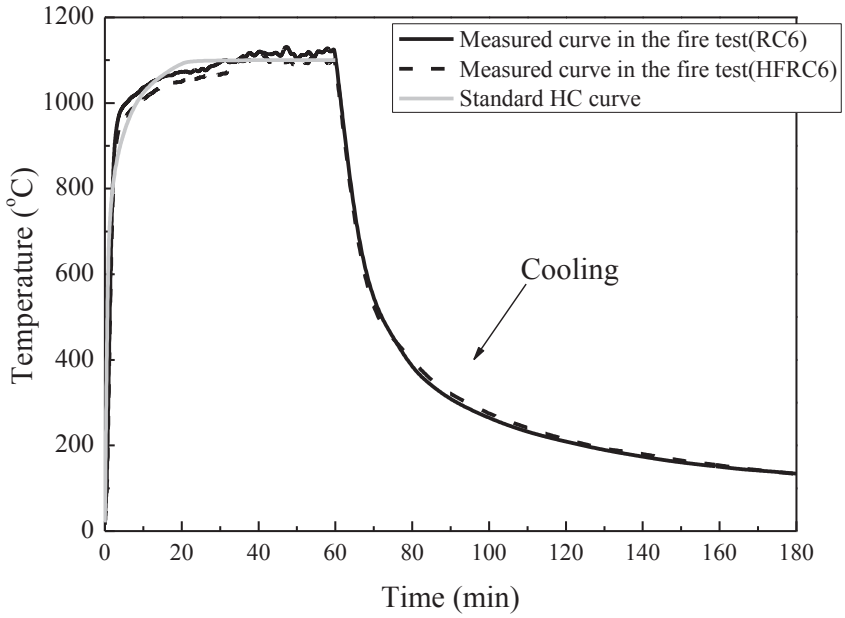


**Fig.4.** Standard HC curve and the measured temperature curves from the fire tests

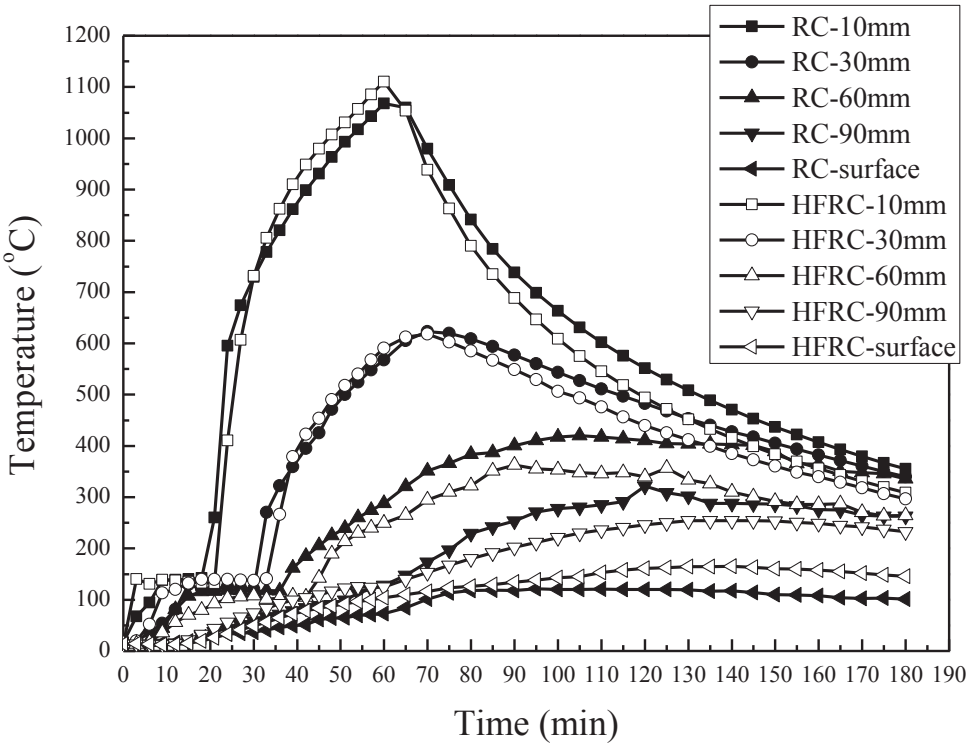


**Fig.5.** Temperature histories at different depths of test specimens from the heating surface during the fire tests

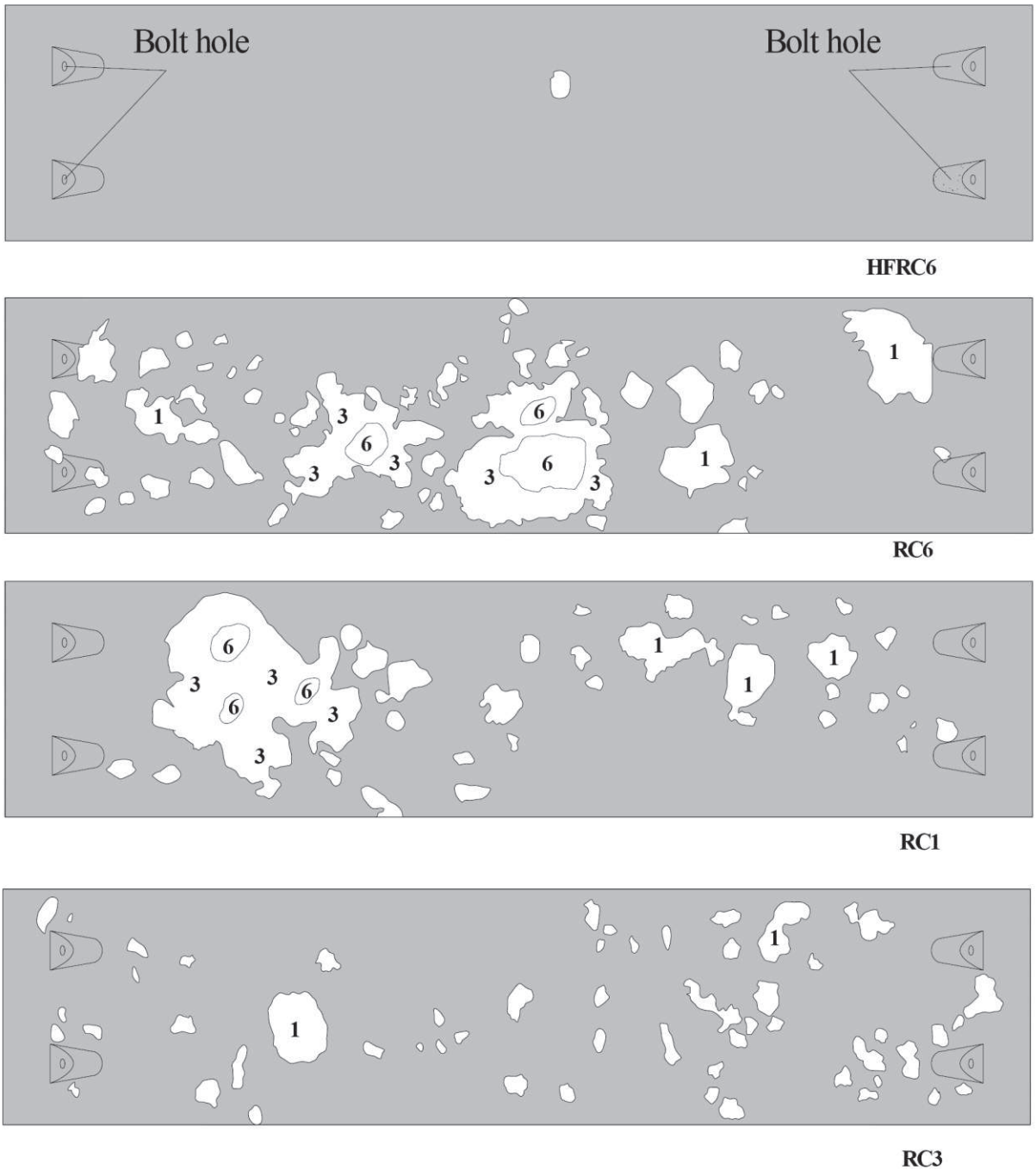


**Fig.6.** Contours of spalling distributions for RC and HFRC segments after fire exposure

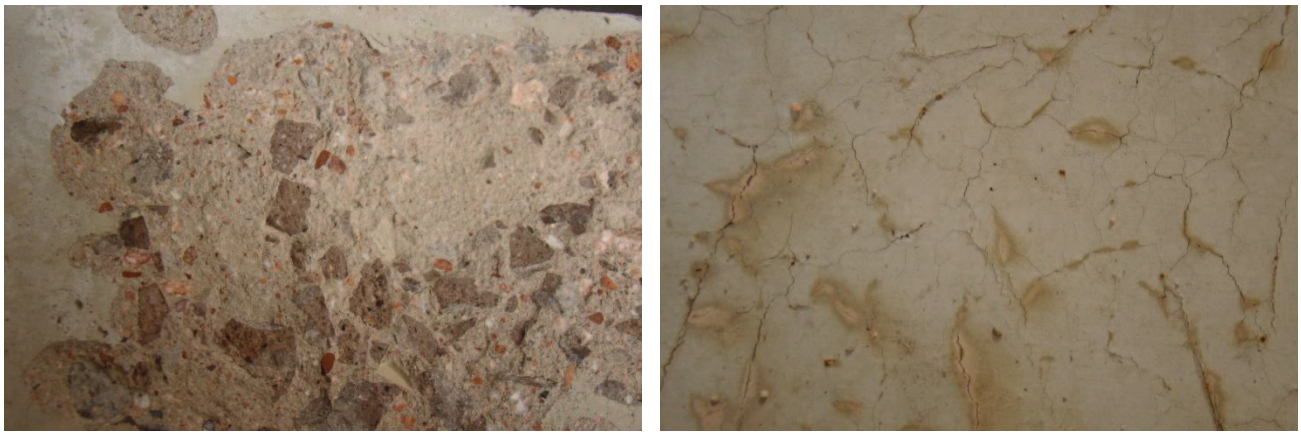

(a) RC segment (b) HFRC segment

**Fig.7.** Comparison of severity of spalling between RC and HFRC segments after fire exposure

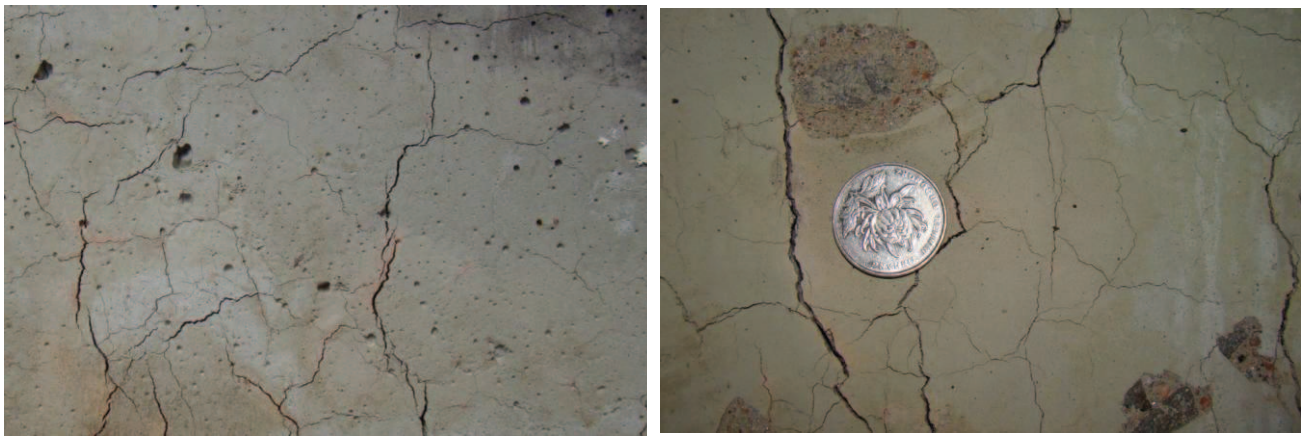

Side face Heated face

(a) RC segments

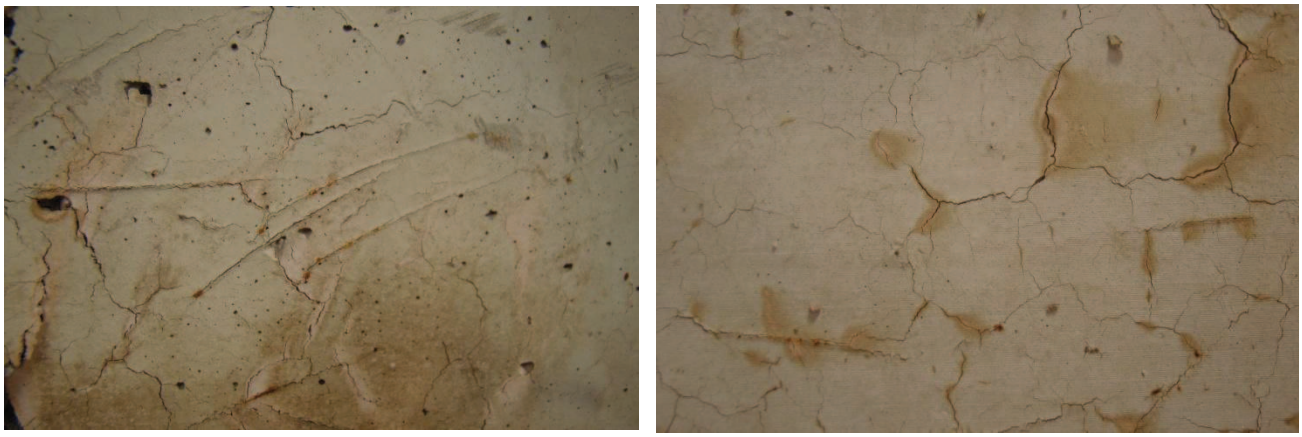

Side face Heated face

(b) HFRC segments

**Fig.8.** Temperature cracks of RC and HFRC segments under LC1 after fire exposure

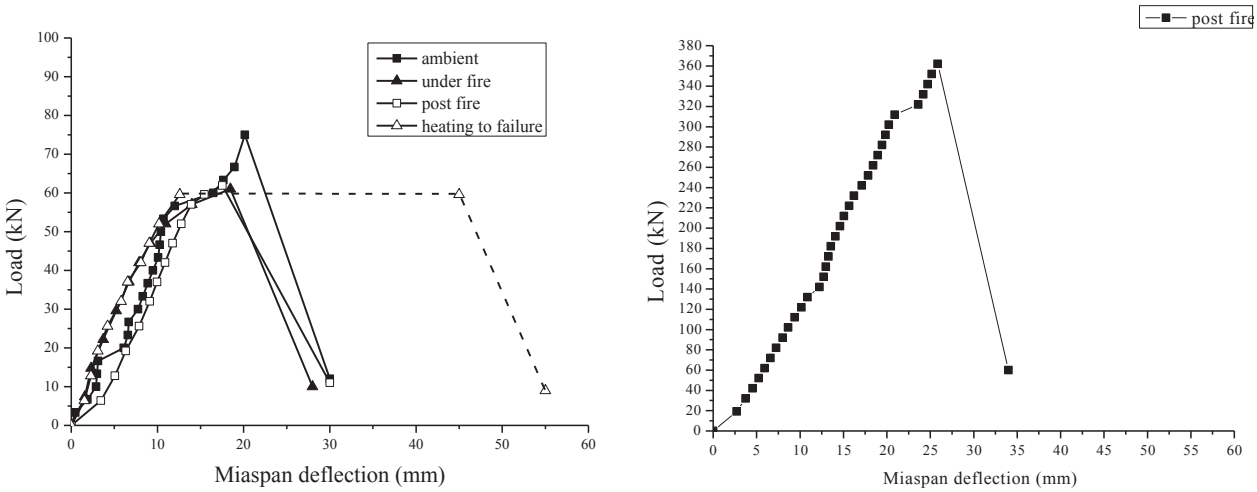


(a) Free sliding BC1 ($R_H$=0) (b) Fixed pins BC2 ($d_H$=0)

**Fig.9.** Vertical load vs. mid-span deflection curves for RC specimens under positive bending moment loading

(a1) RC0, Ambient, free slide ($R_H$=0) (a2) RC1, Under fire, free slide ($R_H$=0)

(a3) RC5, Post fire, free slide ($R_H$=0) (b) RC4, Post fire, fixed pin ($d_H$=0)

**Fig.10.** Failure modes of RC specimens under positive (sagging) moment loading

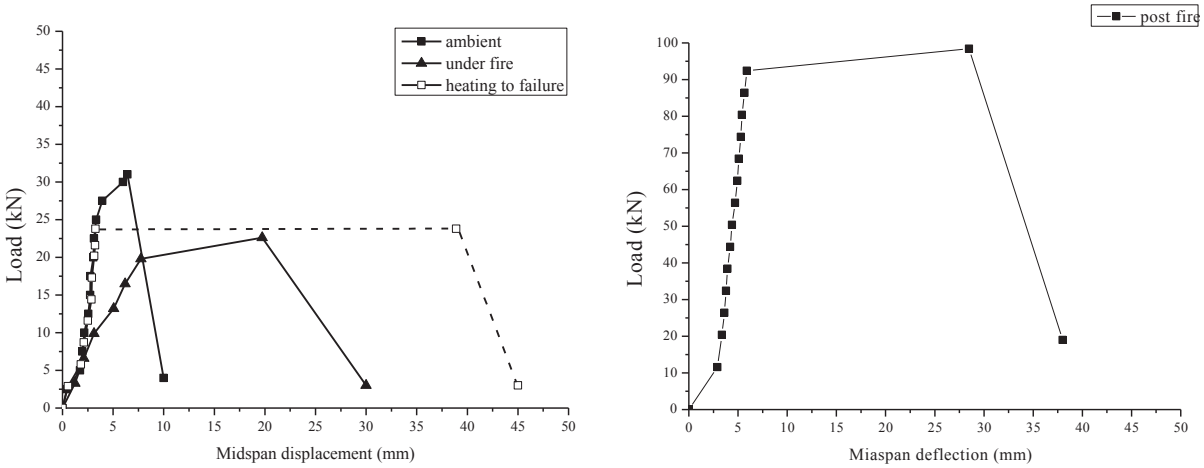


(a) Free sliding BC1 ($R_H$=0) (b) Fixed pins BC2 ($d_H$=0)

**Fig.11.** Vertical load vs. mid-span deflection curves for HFRC specimens under positive bending moment loading

(a1) HFRC0, Ambient, free slide ($R_H$=0) (a2) HFRC1, Under fire, free slide ($R_H$=0)

(a3)HFRC5, Post fire, free slide ($R_H$=0) (b) HFRC4, Post fire, fixed pin ($d_H$=0)

**Fig.12.** Failure modes of HFRC specimens under positive moment loading

(a) Steel fiber failure uner mechancial loading

(b) Steel fiber failure under thermal-mechnical loading

**Fig.13.** Comparison of steel fiber failures between mechanical load test under ambient temperature and fire endurance test

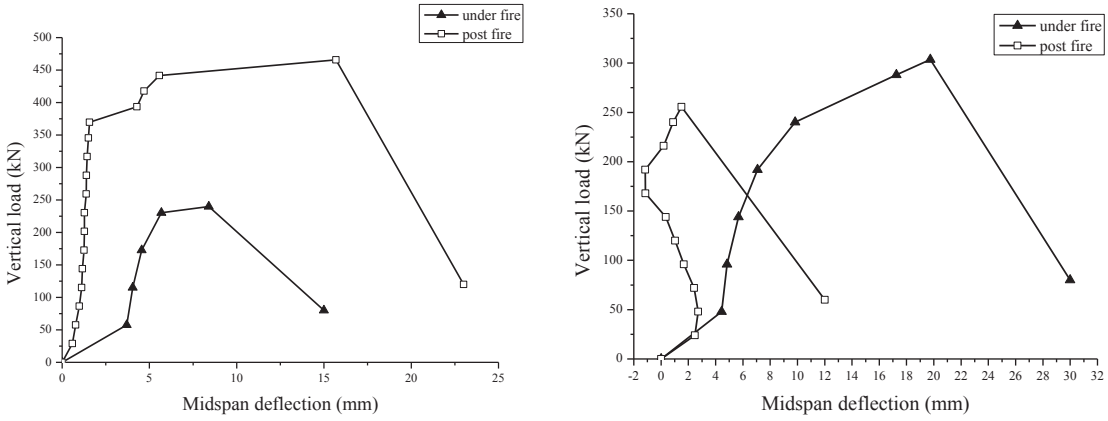


(a) RC ($P_v/R_H=1.2$)

(b) HFRC ($P_v/R_H=1.2$)

**Fig.14.** Vertical load vs. mid-span deflection for hogging moment loading cases

(a) RC2 ($P_v/R_H=1.2$,***under fire***)

(b) RC6 ($P_v/R_H=1.2$,***post fire***)

(c) HFRC2 ($P_v/R_H$=1.2,***under fire***) (d) HFRC6 ($P_v/R_H$=1.2,***post fire***)

**Fig.15.** Failure modes for hogging moment loading cases

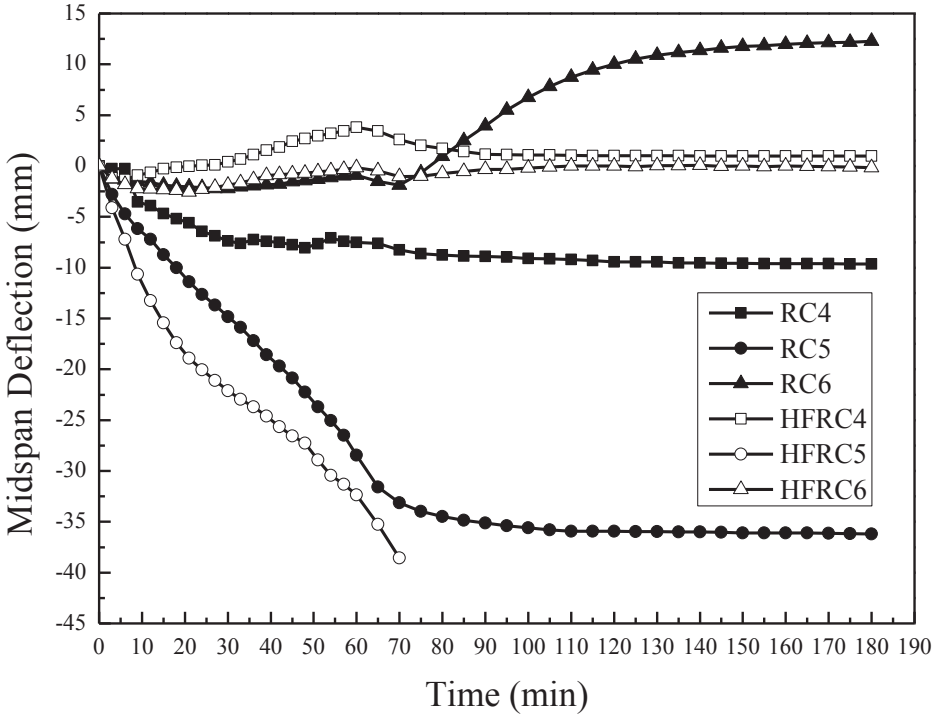


**Fig.16.** Thermal-induced mid-span deflection histories during heating and cooling phases under an initial service load

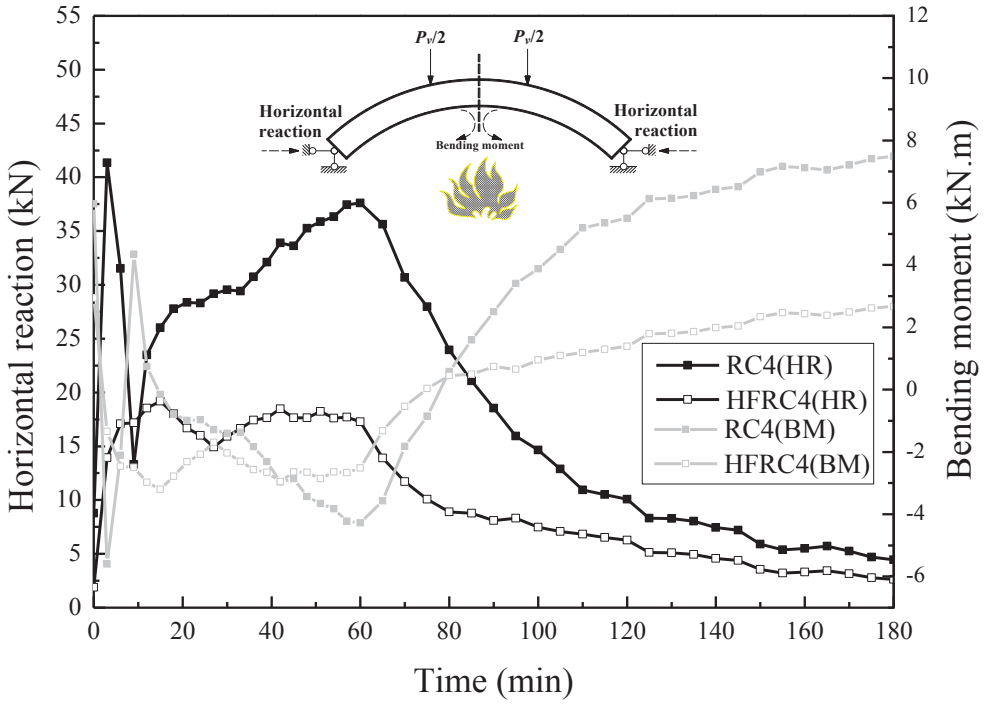


**Fig.17.** Development of horizontal reaction at the supports and bending moment at the central section during heating and cooling phases